Acta Crystallographica Section B
Structural Science
ISSN 0108-7681

Conformational polymorphism in a Schiff-base macrocyclic organic ligand: an experimental and theoretical study

Leonardo Lo Presti,[a]* Raffaella Soave,[b] Mariangela Longhi[a] and Emanuele Ortoleva[a]

[a]Dipartimento di Chimica Fisica ed Elettrochimica, Università degli Studi di Milano, Via Golgi 19, 20133 Milano, Italy, and [b]CNR-ISTM, Istituto di Scienze e Tecnologie Molecolari, Via Golgi 19, 20133 Milano, Italy

Correspondence e-mail: leonardo.lopresti@unimi.it

Received 28 April 2010
Accepted 23 July 2010

Polymorphism in the highly flexible organic Schiff-base macrocycle ligand 3,6,9,17,20,23-hexa-azapentacyclo(23.3.1.1^{11,15}.0^{2,6}.0^{16,20})triaconta-1(29),9,11,13,15(30),23,-25,27-octaene (DIEN, $C_{24}H_{30}N_6$) has been studied by single-crystal X-ray diffraction and both solid-state and gas-phase density functional theory (DFT) calculations. In the literature, only solvated structures of the title compound are known. Two new polymorphs and a new solvated form of DIEN, all obtained from the same solvent with different crystallization conditions, are presented for the first time. They all have $P\bar{1}$ symmetry, with the macrocycle positioned on inversion centres. The two unsolvated polymorphic forms differ in the number of molecules in the asymmetric unit Z', density and cohesive energy. Theoretical results confirm that the most stable form is (II°), with $Z' = 1.5$. Two distinct molecular conformations have been found, named '*endo*' or '*exo*' according to the orientation of the imine N atoms, which can be directed towards the interior or the exterior of the macrocycle. The *endo* arrangement is ubiquitous in the solid state and is shared by two independent molecules which constitute an invariant supramolecular synthon in all the known crystal forms of DIEN. It is also the most stable arrangement in the gas phase. The *exo* form, on the other hand, appears only in phase (II°), which contains both the conformers. Similarities and differences among the occurring packing motifs, as well as solvent effects, are discussed with the aid of Hirshfeld surface fingerprint plots and correlated to the results of the energy analysis. A possible interconversion path in the gas phase between the *endo* and the *exo* conformers has been found by DFT calculations; it consists of a two-step mechanism with activation energies of the order of 30–40 kJ mol^{-1}. These findings have been related to the empirical evidence that the most stable phase (II°) is also the last appearing one, in accordance with Ostwald's rule.

1. Introduction

Polymorphism is the ability of a solid material to exist in more than one crystal structure (McCrone, 1965; Bernstein, 2002). Different polymorphs exhibit different physicochemical properties, such as density, melting point, hygroscopicity and solubility, to mention but a few. For this reason it would be highly desirable, especially in pharmaceutical research, to know how to obtain a specific crystal structure or how to avoid the undesired ones. Moreover, polymorphism has attracted a great deal of interest in the last decades as a crucial topic in crystal engineering (Trask *et al.*, 2005; Braun *et al.*, 2008) as, according to Bernstein (1993), '*the existence of polymorphic crystal structures provides a unique opportunity to study*

structure–property relationships, since the only variable among polymorphic forms is that of structure, and variation in properties must be due to differences in structure'.

Nevertheless, this phenomenon is still not well understood, *i.e.* it is practically impossible to know in advance if a change in the crystallization procedure (solvent, concentration, cooling rate, stirring conditions, presence of impurities) will result in a different crystal structure or not. It is significant that a new polymorph of the simple maleic acid was found 124 years after the first crystal form of this substance was studied (Day *et al.*, 2006). This problem was well known for a long time; in the 1960s, McCrone (1965) stated: '*It is at least this author's opinion that every compound has different polymorphic forms, and that, in general, the number of forms known for a given compound is proportional to the time and money spent in research on that compound*'.

In the last decade, several attempts have been made to predict *ab initio* the crystalline structure of simple organic compounds (Day *et al.*, 2005, 2009; Motherwell *et al.*, 2002; Lommerse *et al.*, 2000). The possibility of predicting a crystal structure directly from the molecular connectivity would be very helpful in assessing the probability of occurrence of polymorphs with specific properties, even before synthesizing the desired compound (Day *et al.*, 2009). During the last blind test on crystal structure prediction (Day *et al.*, 2009), for the first time a group reached the goal to correctly predict all the proposed crystal structures (Neumann *et al.*, 2008). This was certainly an impressive result, but it is worth noting that all the substances examined in this test consisted of small and relatively rigid molecular moieties. Clearly, when a higher number of conformations with quite similar energies are accessible to the compound at ordinary temperatures, conformational polymorphism is to be expected and the prediction of the experimental crystal structure may become a very difficult task.

In the present work a detailed analysis, both experimental and theoretical, on the conformational polymorphism observed in 3,6,9,17,20,23-hexa-azapentacyclo(23.3.1.-$1^{11,15}.0^{2,6}.0^{16,20}$)triaconta-1(29),9,11,13,15(30),23,25,27-octaene (hereinafter, DIEN), is proposed. DIEN is an isomeric form of a hexa-aza 24-membered ring system belonging to the class of tetra-Schiff base macrocyclic organic ligands (Adams *et al.*, 1987; Drew, 1980). The latter compounds have attracted a great deal of interest during the last decades as synthons for tyrosinase model systems (Menif *et al.*, 1990; Martell *et al.*, 1997; Ma *et al.*, 2002; Utz *et al.*, 2003). Actually, tetra-Schiff base dinuclear Cu^{I} complexes can coordinate O_2, promoting the regioselective oxidation of organic substrates (Martell *et al.*, 1997) or even of the ligand itself (Menif *et al.*, 1990). In particular, DIEN is obtained by condensation of 1,3-phthalaldehyde with diethylenetriamine (DETA) and was studied for a long time by means of both spectroscopic and crystallographic techniques (Menif *et al.*, 1990; Adams *et al.*, 1991). There is evidence (Adams *et al.*, 1991) that in solution it exists as a mixture of two constitutional isomers in equilibrium: the first is the title compound and the second is its 'larger' form, 3,6,9,17,20,23-hexa-azatricyclo(23.3.1.$1^{11,15}$)triaconta-1(29),2,-9,11(30),12(13),14,16,23,25,27-decaene (hereinafter, DIEN2: see Fig. 1). With respect to DIEN, DIEN2 lacks the imidazolidine rings and bears two $=N-(CH_2)_2-NH-(CH_2)_2-N=$ groups which can act as tridentate ligands towards a metal centre. Within coordination complexes, only the DIEN2 form of the ligand was observed both in solution and in the solid state (Menif *et al.*, 1990; Adams *et al.*, 1991; Ma *et al.*, 2002; Utz *et al.*, 2003), while the crystallization of the ligand alone seems to invariably lead to DIEN (Menif *et al.*, 1990; Adams *et al.*, 1991). However, it has to be mentioned that the crystal structure of a Ba complex with a methyl-substituted analogue of DIEN was reported several years ago (Drew, 1980).

Owing to its high number of conformational degrees of freedom, this system appears to be a test case to investigate the relationships between the observed packing and the conformation(s) adopted by the individual molecular moieties in the bulk. In this work geometrical information obtained from single-crystal X-ray experiments was supported and supplemented by periodic/gas-phase DFT calculations, with the aim of:

(i) investigating the energetics of the molecular self-recognition process, *i.e.* separating out the main contributions to the lattice energy, and

(ii) gaining insight into the interplay among structure, conformation and packing of DIEN.

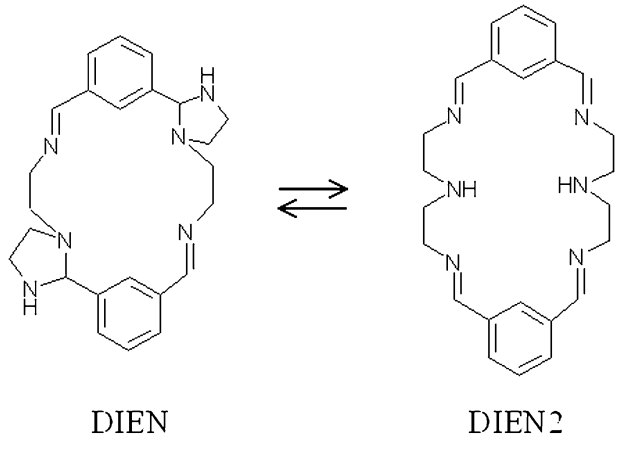

Figure 1
Conversion equilibrium between the DIEN and the DIEN2 forms of $C_{24}H_{30}N_6$ in solution.

2. Methods

2.1. Synthesis

The synthesis of DIEN was carried out according to Menif & Martell (1989) and Menif *et al.* (1990). 1,3-Phthalaldehyde (97%, ACS Reagent Aldrich, 15 mmol) was dissolved in 250 ml of CH_3CN and slowly dropped for 1 h 30 min in a solution of 1.6 ml of DETA in 400 ml of CH_3CN. A white solid appeared after 15 h; the suspension was then filtered on a 0.45 µm Durapore (Millipore) filter. After synthesis, the

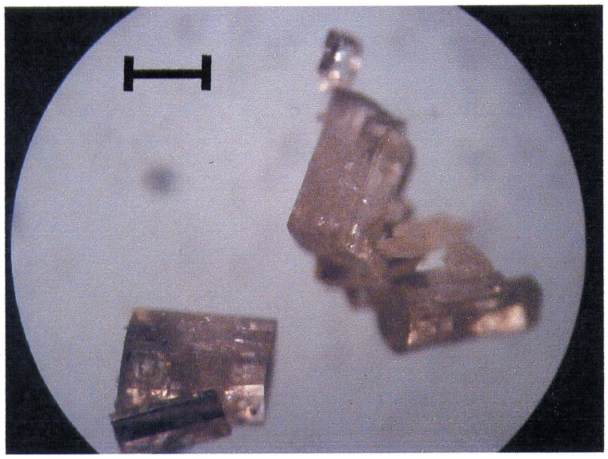

(*a*)

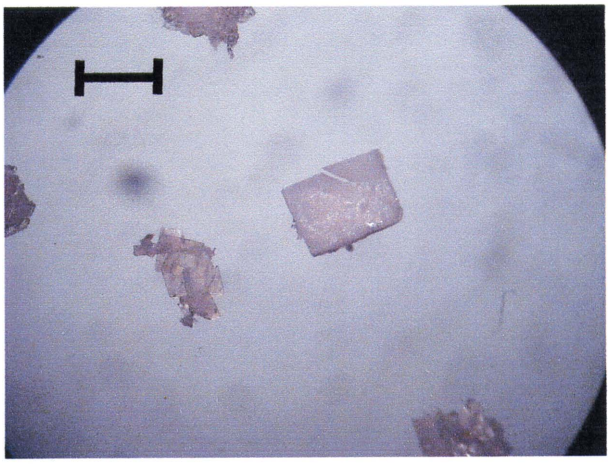

(*b*)

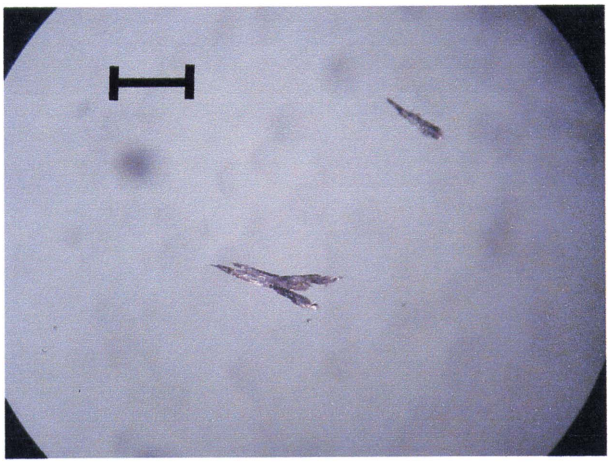

(*c*)

Figure 2
Samples of the three DIEN crystal forms discussed in the present work as viewed with a Zeiss (STEMI DRC) microscope (40× magnification). (*a*) Form (II°), from the first batch of the material (December 2008). The horizontal bar in the photograph roughly corresponds to 720 µm. (*b*) Form SOLV, from the second batch of the material (April 2009). The bar corresponds to ∼ 630 µm. (*c*) Form (I), from the second batch of the material. Same scale as (*b*). This figure is in colour in the electronic version of this paper.

following purification procedure was carried out a total of four times: the product was dissolved in warm CH_3CN (excess):CH_2Cl_2 and then left to cool down again to room temperature. The white precipitate was filtered using a 0.45 µm Durapore (Millipore) filter. Eventually, the solid material was left bathed in the mother solution.

2.2. Single-crystal X-ray experiments

The Kofler notation (Kofler & Kofler, 1954) has been used throughout the paper to identify the new crystal forms. According to this notation, the polymorphs are identified by Roman numerals with melting points in decreasing order. The '°' symbol marks the most stable form. On the contrary, the solvated form is named SOLV hereinafter. It should be stressed that the latter cannot be considered, strictly speaking, as a true polymorphic form of DIEN, as it contains guest chemical species in the unit cell. Both recently and in the past, especially in the pharmaceutical literature, solvated crystal forms of organic substances were referred to as 'pseudopolymorphs'. However, it should be noted that this term has been recently criticized (Bernstein, 2002; Seddon, 2004) as in the last decades the same word 'pseudopolymorphism' has been adopted to indicate a huge variety of phenomena, including second-order phase transitions, desolvation, dynamic isomerism, mesomorphism, and so on. Threlfall (1995) also pointed out that, as solvated and unsolvated phases of the same substance are constitutionally different, they cannot be classified as 'polymorphs' by any definition. Accordingly, in this work we keep distinct the discussion on crystal packing and energetics of the SOLV phase with respect to the other two unsolvated ones, (II°) and (I), and compare the former with the other solvated forms of DIEN reported in the literature.

2.2.1. DIEN polymorph (II°). The first synthesis was carried out in December 2008. A suspension of the title compound in CH_3CN (excess):CH_2Cl_2 rested for a couple of days at room temperature in a crystallizer covered with a watch glass, with the solvent left free to evaporate slowly. At the beginning of the crystal growing process, the majority of the material was composed by thin and very small white needles. After ∼ 48 h larger and regular prisms appeared (Fig. 2*a*), while the number of needle-like crystals was found to be considerably reduced. After a preliminary selection at the stereomicroscope, a fragment cut from a large prism was employed for the X-ray analysis.

2.2.2. SOLV. Owing to the poor overall quality of the needle-shaped crystals obtained after the first crystallization described above we tried to obtain a larger amount by rapidly cooling the mother solution. The synthesis process was repeated 4 months after (April 2009) and the warm reaction mixture of the title compound in CH_3CN (excess):CH_2Cl_2 was abruptly cooled by placing it in a refrigerator at $T = 277$ K just at the end of the purification procedure. A white precipitate was immediately obtained. It was composed of several, unexpected, very small plate-like transparent crystals (Fig. 2*b*) and a much lower number of thin needles of habit analogous

Table 1
Experimental table for DIEN samples.

For all structures: triclinic, $P\bar{1}$. Experiments were carried out at 293 K with Mo $K\alpha$ radiation using a Bruker AXS Smart diffractometer. Data collection used ω scans. Empirical absorption correction (using intensity measurements), *SADABS*2007/4. Refinement was with 0 restraints. H atoms were treated by a mixture of independent and constrained refinement.

	(II°)	(I)	SOLV
Crystal data			
Chemical formula	$C_{24}H_{30}N_6$	$C_{24}H_{30}N_6$	$3C_{24}H_{30}N_6{\cdot}2C_2H_3N{\cdot}0.68O$
M_r	402.54	402.54	1300.67
a, b, c (Å)	9.697 (1), 12.243 (1), 13.937 (1)	9.8236 (3), 9.9337 (3), 12.1088 (4)	12.237 (1), 12.563 (1), 13.009 (1)
α, β, γ (°)	87.182 (2), 81.257 (2), 82.062 (2)	92.421 (3), 81.230 (3), 72.989 (3)†	87.378 (3), 68.153 (3), 79.441 (3)
V (Å^3)	1618.9 (3)	1112.00 (6)	1824.4 (3)
Z, Z' ‡	3, 1.5	2, 1	3, 1.5
$F(000)$	648	432	697.6
D_x (g cm^{-3})	1.239	1.202	1.185
Measured m.p.§ (K)	440.5 (5)	452.5 (5)	417.0 (5)
μ (mm^{-1})	0.08	0.07	0.07
Crystal size (mm)	0.23 × 0.20 × 0.05	0.70 × 0.20 × 0.20	0.23 × 0.15 × 0.03
Data collection			
T_{min}, T_{max}	0.936, 0.943	0.944, 1.000	0.850, 1.000
No. of measured, independent and observed [$I > 2\sigma(I)$] reflections	48 844, 7448, 3646	24 298, 5093, 2892	22 307, 8389, 2729
R_{int}	0.109	0.033	0.101
Refinement			
$R(F)$, $R(F^2)$,¶ S	0.054, 0.114, 1.01	0.043, 0.102, 0.95	0.056, 0.107, 0.87
No. of reflections	7448	5093	8389
No. of variables (N_v)	419	280	449
$\Delta\rho_{max}$, $\Delta\rho_{min}$ (e Å^{-3})	0.30, −0.21	0.15, −0.13	0.20, −0.14
N_{gt}/N_v	8.7	10.3	6.1
Extinction coefficient	0.004 (1)	0.015 (2)	0.0033 (8)

† In this table the cell setting of phase (I) differs with respect to that reported in the deposited CIF file to make easy the comparison among the three structures. ‡ Z is defined as the number of formula units in the unit cell, whereas Z', strictly speaking, is given by Z divided by the number of independent general positions for a given space group (see also http://www.dur.ac.uk/zprime/). Being aware of the flaws that could be involved in such a definition, the 'formula unit' indicates here an entire DIEN molecule, whereas Z' expresses the number of formula units in the asymmetric unit [*i.e.* as the asymmetric unit contains two or three half-molecules, $Z' = 3 \times 0.5 = 1.5$ in forms (II°) and SOLV, and $Z' = 2 \times 0.5 = 1$ in form (I)]. § Measured with SMP3 melting point apparatus from Stuart Scientific. ¶ Evaluated for the reflections active in the refinement, *i.e.* the N_{gt} data with $I > 2\sigma(I)$.

to those formerly observed (Fig. 2*c*). We then decided to analyze the crystal structure of the newly appearing phase. Part of the material floating throughout the solvent was taken with a Pasteur pipette and screened under polarized light with a stereomicroscope. After testing some twinned and poorly diffracting crystals a thin-plate sample was eventually selected for the X-ray analysis.

2.2.3. DIEN polymorph (I). Several needle-shaped crystals (Fig. 2*c*) from both the batches described above (*i.e.* December 2008 and April 2009) were examined carefully, at both the stereomicroscope and the diffractometer. Owing to their small dimensions and polycrystalline nature, it was difficult to find a sample suitable for an accurate X-ray diffraction experiment. Eventually, in the batch obtained by abrupt cooling, a thin fragment ($0.7 \times 0.2 \times 0.2$ mm^3) cut from the extremity of a longer individual was found to be adequate for the X-ray analysis.

Details of the room-temperature single-crystal X-ray experiments are summarized in Table 1. In all cases, a three-circle Bruker AXS Smart Apex diffractometer equipped with an Apex II CCD detector was employed. Owing to the low crystal symmetry, an entire sphere of data with the highest possible redundancy was collected for all samples. The data were empirically corrected for beam anisotropy and an isotropic extinction correction was applied in the final least-squares model. Full details on the data collection strategies and crystal structure refinements are available in the supplementary material.[1]

It should be noted that, just after the synthesis, form (I) (needles) was predominant, but after a couple of days, during which the solid material was left in the reaction solvent, a large amount of form (II°) (prisms) appeared. However, no interconversion among the two polymorphs and the solvated phase, or any other kind of structural transformations, were observed over a period of several (12–16) months, provided that the material was removed from the solution. We noted that the large prisms corresponding to the crystal form (II°), kept at room temperature, slowly turned yellow.[2] In April 2009 we performed an extensive data collection on another sample (pale-yellow coloured) of form (II°) from the December 2008 batch (see above). We definitely found the same crystal structure as reported here for this polymorph, even if we

[1] Supplementary data for this paper are available from the IUCr electronic archives (Reference: PS5007). Services for accessing these data are described at the back of the journal.
[2] Recrystallization of the yellowish material from CH_3CN:CH_2Cl_2 leads again to white crystals (needles at first which were subsequently replaced again by prisms).

noted that the data quality, in terms of reflection intensity and shape, became slightly worse. We attributed such a deterioration to the crystallinity loss of the material over time. We suppose that the latter may be due, in turn, to slow reaction of the crystal with atmospheric oxygen or with moisture in the air, rather than to some kind of photochemical processes caused by visible light, as conservation of the sample in the dark in a cupboard did not prevent the material from slowly deteriorating.

2.3. Theoretical calculations

Owing to the intrinsic difficulty of locating H atoms directly from X-ray diffraction data, the H-atom positions for each independent molecule in the asymmetric unit were optimized in the gas phase at the DFT B3LYP (Lee *et al.*, 1988; Becke, 1993) 6-311++G(p,d) theory level before carrying out any packing analysis and energy calculation (see §§3.2.1 and 3.3), with the coordinates of all the C and N atoms kept frozen at their experimental values. Both the *GAUSSIAN*03 (Frisch *et al.*, 2004) and the *GAUSSIAN*09 (Frisch *et al.*, 2009) program versions were employed for the gas-phase calculations. These partially relaxed geometries were adopted to perform single-point periodic simulations, with the same Hamiltonian, to evaluate the cohesive crystal energies of the three newly discovered crystal forms of DIEN. *CRYSTAL*06 software (Dovesi *et al.*, 2006) was used for the solid-state calculations, with a 6-31G(d) basis set formerly optimized for organic crystals (Gatti *et al.*, 1994; Spackman & Mitchell, 2001). Details concerning computational strategies and cost can be found in the supplementary material.

The cohesive energy of the two unsolvated polymorphs (II°) and (I) was evaluated as

$$\begin{aligned} E_{\rm cohesive} &= E_{\rm bulk} - \sum_{i=1,n} E_{\rm iso}(i) - \sum_{i=1,n} E_{\rm rel}(i) + \sum_{i=1,n} E_{\rm BSSE}(i) \\ &= E_{\rm b} - \sum_{i=1,n} E_{\rm rel}(i) + \sum_{i=1,n} E_{\rm BSSE}(i), \end{aligned} \quad (1)$$

where $E_{\rm bulk}$ is the total energy of the unit cell, $E_{\rm iso}(i)$ is the energy of each ith isolated molecule which keeps its solid-state conformation, $E_{\rm rel}(i)$ is the relaxation energy (it is a negative term accounting for the difference between the energies of an isolated molecule in its solid-state and relaxed conformations) and $E_{\rm BSSE}(i)$ is the correction owing to the basis set superposition error (BSSE) of the ith molecule. All sums run over the n molecules in the unit cell. The difference among $E_{\rm bulk}$ and all the $E_{\rm iso}(i)$ terms gives the crystal binding energy $E_{\rm b}$, *i.e.* the overall gain in energy upon lattice formation. An analogue formula was recently employed to evaluate the cohesive energy of less complex molecular crystals (Civalleri *et al.*, 2007; Lo Presti *et al.*, 2009). More details concerning the evaluation of the $E_{\rm BSSE}$ and $E_{\rm rel}$ terms in (1) are available in the supplementary material.

It should be noted that this model for the crystal cohesive energy cannot be strictly related to thermodynamic quantities such as the sublimation enthalpies at 0 K, $\Delta_{\rm sub}H^0(0)$, because it lacks two important contributions: the vibrational zero-point energy of the molecules in the crystalline state and the dispersion (van der Waals) energy (van Mourik & Gdanitz, 2002) at large separations. In particular, the latter term is known to be entirely missed by ground-state DFT methods (Dobson *et al.*, 2001), because the LDA/GGA schemes cannot account for correlations between distant electrons when these differ from those of a uniform (or near-uniform) electron gas. However, in this work we are interested in ranking the crystal cohesive energy on a relative scale, *i.e.* to identify the most stable polymorph among the new structures found, not in evaluating the absolute crystal energy. Therefore, dispersion terms were estimated by atom–atom summation of empirically derived potentials (Williams & Cox, 1984) among different molecules over the crystal. Then, the van der Waals estimates were used to provide a tentative correction to the quantum mechanical crystal cohesive energy. More details are available in the supplementary material.

The interaction energy of relevant solid-state molecular pairs in the newly discovered polymorphs was evaluated by means of *GAUSSIAN*03 gas-phase calculations at the 6-311++G(p,d) B3LYP theory level, adopting the same geometry as in the condensed phase. The counterpoise (CP) technique (Boys & Bernardi, 1970) was employed to estimate the amount of BSSE correction. Eventually, the energy barrier for the conformational interconversion between the 'imine *endo*' and the 'imine *exo*' arrangements was estimated by a transition-state optimization in the gas phase; full details can be found in the supplementary material. The smaller 6-31G(d) basis set, together with the same DFT B3LYP Hamiltonian, was employed for evaluation of the interconversion barrier.

2.4. Melting-point measurements

Melting points were also determined for all the three newly discovered crystal forms with an SMP3 melting point apparatus from Stuart Scientific. In all cases variable heating rates (1–5 K min^{-1}) were employed. For all the three crystal forms, after the fusion took place and the temperature was brought back to ambient temperature, the material appeared as a shapeless yellow solid.

3. Results and discussion

Fig. 3 reports the atom-numbering scheme. For both forms (II°) and SOLV, the asymmetric unit is composed of three half molecules, which are marked in the following discussion by *A*, *B* and *C* according to their crystal environment. In each crystal form we labelled '*A*' as the molecule closest to the origin and '*B*' as the independent moiety closest to '*A*', while molecule '*C*' in both SOLV and (II°) has its centre of mass in 0.5, 0.5, 0.5 (fractional coordinates). The molecule to which an atom belongs is uniquely identified by appending the molecule label to the atom label (*e.g.* atom C1*A* belongs to molecule *A*, whereas atom C1*B* has the same connectivity as C1*A* but in molecule *B*, and so on). As regards form (I), the asymmetric unit contains only two half molecules, *i.e.* it lacks the *C* molecule. For the sake of clarity, the same labelling scheme

was also applied to the two other solvated forms of DIEN reported in the literature and discussed here.

3.1. Molecular conformation

In this section the geometries of all the independent molecules in all the known DIEN phases are discussed, including the two solvated forms previously reported in the literature (Menif *et al.*, 1990; Adams *et al.*, 1991). Analysis of the similarities and differences in crystal packing is given in §§3.2.1 and 3.4 for the unsolvated and solvated structures. Hereinafter we will refer to the two forms retrieved from the above papers using their Cambridge Structural Database (CSD) refcodes, *i.e.* SOVJUI for the dichloromethane solvate (Adams *et al.*, 1991) and KIGVEB for the methanol solvate (Menif *et al.*, 1990). A more detailed and extended discussion on this topic can be found in the supplementary material. It was found that, on average, the root mean-square deviations (r.m.s.d.s) of the C—N bond distances and angles with respect to the corresponding weighted mean values are of the order of 10^{-2} Å and 10^{0}°. Such variability in bond angles is likely to be a consequence of the relative flexibility of the macrocycle, and it is particularly evident when molecule *C* in (II°) is compared with each other independent DIEN unit, no matter the crystal structure to which it belongs. This is due to the important conformational differences relative just to molecule *C* in (II°).

When backbone torsions are considered, both similarities and differences emerge. In Fig. 4 the absolute values of the torsion angles of all the 12 independent DIEN units found in the five known DIEN crystal forms [(II°), (I), SOLV, KIGVEB and SOVJUI] are displayed. The three fragments of major chemical relevance (*i.e.* the imidazolidine, the phenyl and the imine groups) are highlighted by superimposing their molecular schemes on the graphic just above the corresponding labels. It is quite evident that most of the molecules share essentially the same conformation. Only one molecule, namely molecule *C* in phase (II°), marked in the graphic by the full red line, shows a completely different trend of torsion angles with respect to the other 11 independent units. In other words, it adopts a different conformation in the solid state. This is confirmed by a closer inspection of individual torsion angle values. For instance, in (II°) the imine torsion angle $|\tau$(C4—C5—C7—N1)| is as large as 166.2 (2), 163.9 (2) and 2.5 (4)° for molecules *A*, *B* and *C*. Such differences are readily explained in Fig. 5, which shows molecules *C* as found in the crystalline forms (II°) and SOLV. On the right (Fig. 5*b*) the most common arrangement of the macrocycle, also shared by molecules *A* and *B* in all the other phases (see Fig. 4), is displayed: it can be seen that the N atoms (N1) of the imine groups are directed inside the major ring ('imine *endo*' arrangement). On the contrary, in the other conformer [molecule *C* in (II°), Fig. 5*a*] the same N atoms are directed outside the macrocycle ring ('imine *exo*' arrangement). As shown in §3.3, this has important consequences on the energetics of the crystal form (II°) with respect to the other unsolvated polymorph.

Some significant differences emerge among the 11 independent macrocycle molecules exhibiting the *endo* conformation, as highlighted in Fig. 4 by small black arrows marking torsion angles that differ by more than ∼20°. These dissimilarities involve torsions such as C7—N1—C8—C9, C2—C1—C12—N2, C6—C1—C12—N2 and C2—C1—C12—N3 (see also Fig. 3), *i.e.* they involve the way in which the various chemically relevant moieties (*i.e.* phenyl, imine and imidazo-

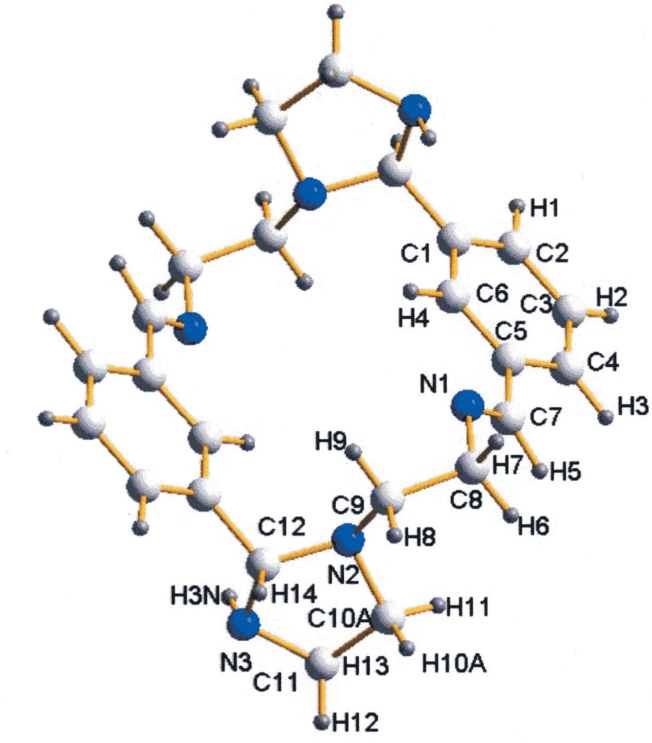

Figure 3
DIEN molecule with atom numbering scheme.

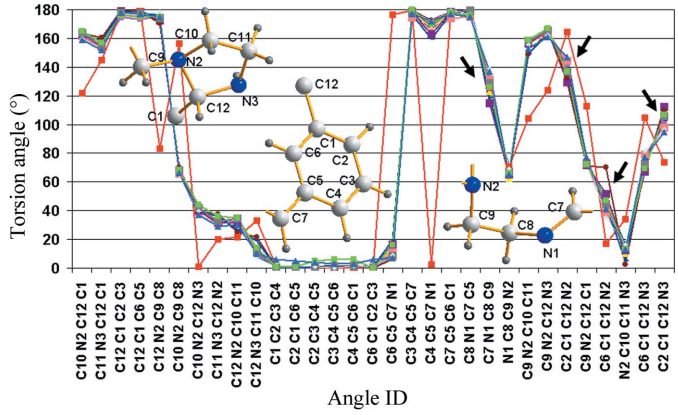

Figure 4
Absolute values of the torsion angles (°) of each of the 12 independent molecules in all crystalline environments of the known DIEN forms. The red line refers to the unique *exo* conformation (see text). Black arrows highlight the angle values of the *endo* conformers discussed in §3.1. Points in the graphic are as large as ∼2.9°, the corresponding estimated standard deviations being considerably lower (on average, from 0.2 to 0.5° for the structures reported in this work and ∼1.5° for the two structures taken from the literature). This figure is in colour in the electronic version of this paper.

lidine), by themselves essentially rigid, are interconnected with each other. However, apart from the above commented exceptions, torsion angles are identical, on average, within a few degrees among all the 11 *endo* conformers. Smaller differences within each of the functional groups are commented in the supplementary material.

3.2. Comparison of the two polymorphic forms: crystal packing

3.2.1. Packing motifs. The conformational differences described earlier provide a rationale to understand conformational polymorphism in DIEN. Generally speaking, this phenomenon occurs when two or more conformers of a given substance pack in different ways in the solid state. In this section the crystal structures of the two polymorphs (II°) and (I) are compared, whereas a discussion on the three solvated forms will be given in detail in §3.4.

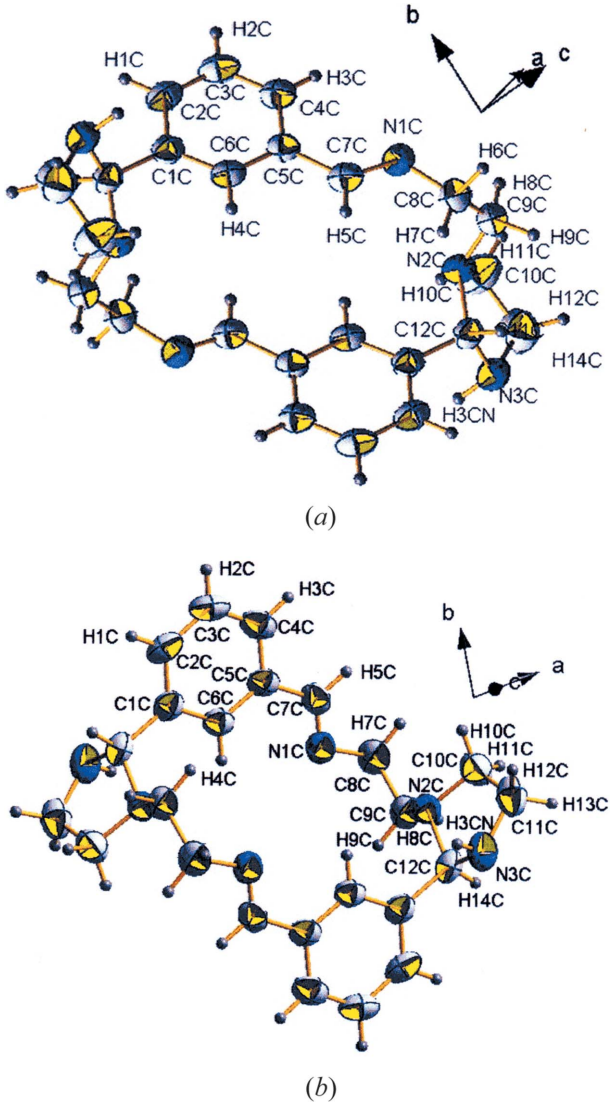

Figure 5
Experimental room-temperature geometry of the two known conformers of DIEN in the solid state. The molecular graphs were realised with the *DIAMOND* program (Brandenburg, 2010), with displacement ellipsoids drawn at the 50% probability level. (*a*) Molecule *C* in the crystal form (II°) (imine *exo*). (*b*) Molecule *C* in the crystal form SOLV (imine *endo*). The latter is the most commonly occurring conformer, as the *endo* arrangement is also adopted by molecules *A* and *B* in all the other known crystal forms of DIEN, including the two solvated structures reported in the literature. This figure is in colour in the electronic version of this paper.

As recently pointed out (Nangia, 2008), it is likely that flexible systems are prone to polymorphism. It should be kept in mind that, eventually, it is the overall gain in energy upon crystallization which dictates the observed crystal form. Especially when distortions from the relaxed gas-phase geometry are available with small energy expenses, *each* molecule is encouraged by the crystal force field to adjust its conformation to make more favourable hydrogen bonds or van der Waals interactions (Nangia, 2008), therefore achieving overall a more favourable crystal cohesive energy. If such geometry changes are relevant it is likely, although not common, that more than one conformer share the same phase, *i.e.* that the phenomenon known as 'conformational isomorphism' may occur (Corradini, 1975). This is precisely the case in the DIEN phase (II°). On the other hand, it is also possible that the chemical units retain the same overall conformation, becoming crystallographically independent at the same time. This implies that some individual geometry adjustments and/or nearly rigid reorientation of at least one molecule take place, as in the case of the DIEN phases (I) and SOLV.

Asymmetries in the structures can also be inferred from the Z' parameter (Table 1), defined as the number of chemical formula units per asymmetric unit. With regard to DIEN, the newly discovered phases have $Z' = 1.5$ [(II°), SOLV] and $Z' = 1$ (I). In the latter case the asymmetric unit contains just one formula unit, but it is composed of *two half* molecules, which each contribute 0.5 to the overall Z' value, whereas in the former crystals the asymmetric unit is composed of *three half* molecules. It is worth noting that very few substances are known with $Z' = 1.5$: as an example, among the purely organic structures deposited in the CSD up to 2000, only 0.22 (2)% were found to have $Z' = 1.5$ (Steiner, 2000). It should be stressed that over the last 9 years this small percentage was reduced even further, now being as low as 0.10% with respect to the overall number of structures deposited in the 2009 CSD release. For the sake of comparison, much more substances (7.8%) are known with two molecules per asymmetric unit.

The main difference in crystal packing between the two unsolvated forms (II°) and (I) is just the presence of a third independent molecule in (II°), labelled as molecule *C*, which adopts the less common *exo* conformation (see §3.1). In Fig. 6 the main packing motifs of both crystal forms are reported and superimposed. In both structures the independent *A* and *B* molecules pile up together along a cell axis [more precisely *b* in (II°) and *c* in (I)]. The macrocycle *A* and *B* units are always tilted with respect to each other and also with respect to the packing direction. Considering the least-squares plane through the largest ring of each independent macrocycle molecule as the main molecular plane, defined by the atom sequence [—C1—C12—N2—C9—C8—N1—C7—C5—C6—]

(and reproduced by the inversion symmetry), it is interesting to note that it is tilted by almost the same amount with respect to the packing axis in both polymorphs. More precisely, the main plane of molecule *A* makes an angle of 51.5° with the *b* axis in polymorph (II°) and 46.9° with the *c* axis in polymorph (I). The same quantities for molecule *B* are as large as 28.9° [form (II°)] and 29.7° [form (I)]. Moreover, the angles between the main planes of molecules *A* and *B* are similar in both polymorphs [22.6° in form (II°) and 18.2° in form (I)], indicating that the mutual orientation of the macrocycles along the respective packing directions is very similar. On the contrary, molecule *C* in polymorph (II°) has a completely different orientation, with its main plane making angles as large as 77.4 and 38.1° with respect to the *b* and *a* cell axes.

Such an arrangement gives rise to alternating *A*, *B*, *A*, *B* stacks over ∼ 12 Å (Fig. 6), which is just the length of the cell axis along the stacking direction (see also Table 1). The two crystal forms share the same *A*, *B*, *A*, *B* motif, with the *A*, *B* molecules being roughly 6 Å apart from each other. In form (II°) the third independent molecule (*C*) intercalates between the parallel columns of units which pack along **b**, pulling them apart along the *c* direction. To visualize more easily the motifs described above, it is useful to approximate with an ellipse the form of the macrocycle as it appears in Fig. 6(*c*) [*i.e.* along the *b* axis of form (II°)]. In this way, two spacing directions can be recognized: the first is roughly perpendicular to the major axis of the ellipse [*i.e.* along **a** in form (II°) and along **b** in form (I)], and the second runs along the direction orthogonal to the minor axis [*i.e.* along **c** in form (II°) and roughly along **a** in form (I)]. From the superposition scheme in Fig. 6(*c*) it is clear that the spacing perpendicular to the major axes should be similar in both crystal forms, while that perpendicular to the minor axes should be greater in form (II°) owing to the presence of the third independent molecule. This is indeed true and it can be seen by inspecting the length of the cell axes (see Table 1): the *a* and *b* unit translations in polymorphs (II°) and (I) are very similar (*a* = 9.97 *versus* *b* = 9.93 Å), both of them being relative to the major axes spacing. On the contrary, the *c* axis in form (II°) is ∼ 41% longer with respect to the *a* axis in form (I) (*c* = 13.94 *versus* *a* = 9.82 Å), as this is the translation period in the direction orthogonal to the minor axes of the macrocycle.

3.2.2. Hirshfeld surface fingerprint plots. Fig. 7 shows the Hirshfeld surface fingerprint plots (Spackman & McKinnon, 2002) of independent molecules in form (II°) and (I). A Hirshfeld surface is defined as the boundary surrounding a given molecule, inside which the promolecular density exceeds that due to any other molecule (McKinnon *et al.*, 1998). In particular, a fingerprint plot displays the fraction of points on the Hirshfeld surface with specific d_i, d_e values, d_i and d_e being the closest distances of nuclei inside and outside the volume enclosed by the surface itself. Such plots are unique for a given crystal structure, and encode information about the intermolecular interactions in the immediate environment of each molecule in the asymmetric unit. In their pioneering work, Spackman & McKinnon (2002) showed some examples of fingerprint plots applied to different polymorphs and even to crystal structures with $Z' > 1$. More recently, this graphical tool has been increasingly applied in the realm of crystal chemistry to compare somewhat related crystal structures. As an example it has been adopted to study solvated forms of hydroquinone (Clausen *et al.*, 2010) and polymorphism in systems such as 1,8-dihydroxyanthraquinone (Rohl *et al.*, 2008), cinacalcet hydrochloride (Braun *et al.*, 2008) and 2-oxopyrrolidineacetamide (Fabbiani *et al.*, 2005). Remarkably, it was also recently applied to structural changes as a function of the external pressure (Fabbiani *et al.*, 2005; Moggach *et al.*, 2006, 2008).

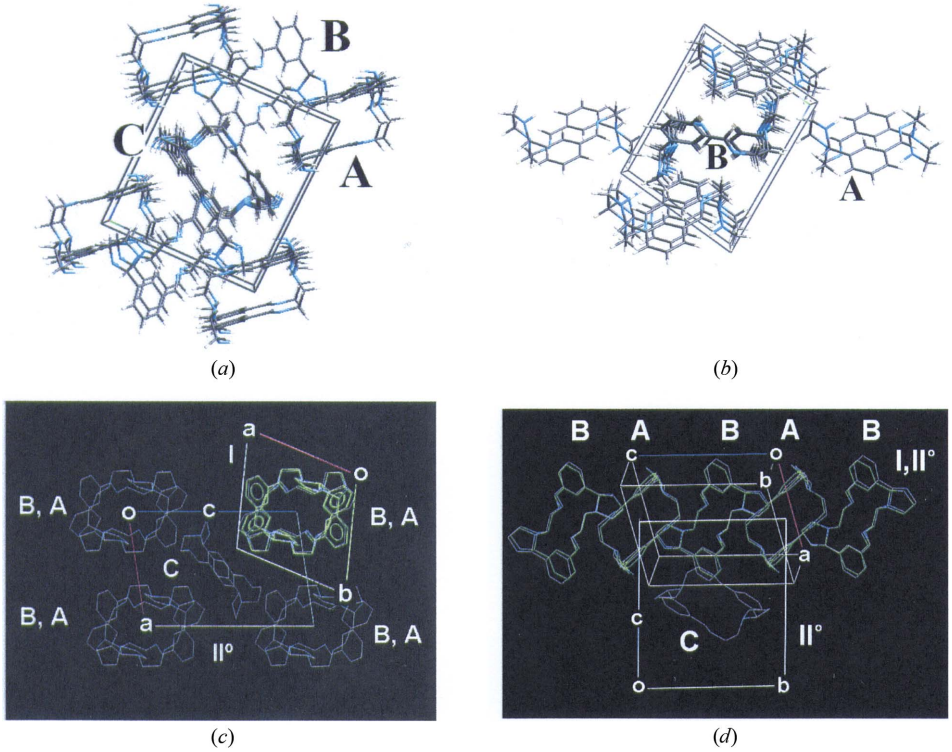

Figure 6
Packing diagrams for polymorphs (II°) and (I) of DIEN. Pictures (*a*) and (*b*) were realized with *Crystal Explorer* 2.1 (Wolff *et al.*, 2007), and (*c*) and (*d*) with *Mercury* CSD 2.2. (*a*) Form (II°) along the *a* axis. (*b*) Form (I), along the *a* axis. (*c*) Superposition of the unit cell contents of form (II°) (perpendicular view of the cell down the *b* axis, grey molecules) and (I) (upper cell, green molecules, along the *c* axis). (*d*) Same as (*c*), viewed down the *a* axis of form (II°) (lower cell). H atoms were omitted for clarity. This figure is in colour in the electronic version of this paper.

In Fig. 7 some common features are evident, namely:

(i) a spike along the main diagonal of the plot, with minimum $d_i + d_e \simeq 2.2$–2.4 Å, which becomes yellow–red at higher $d_i + d_e$ values;

(ii) lateral blue 'wings' at $d_i + d_e \simeq 3.0$ Å [form (II°)] or at $d_i + d_e \sim 3.2$–3.3 Å [form (I)];

(iii) short and sharp lateral blue–green spikes, barely visible in form (I), with minimum $d_i + d_e$ between ~ 2.2 and ~ 2.5 Å in phases (II°) and (I).

Each of these represents a specific packing feature. In particular, (i) indicates short, almost linear, C—H···H—C contacts. The H···H contacts are common in organic crystals owing to the larger number of H atoms with respect to heavier elements, as in the well known case of the linear saturated alkanes (Spackman & McKinnon, 2002): in DIEN, these interactions account for 67.7–72.3% of the total area covered by the various fingerprint plots. Feature (ii) signals the presence of C—H···π interactions involving the phenyl groups. It is worth noting that the 'wings' are more evident for molecules in the crystal form (II°), suggesting that such contacts are, on the contrary, less important in polymorph (I). Closer inspection of the intermolecular contacts reveals that in the latter there are only two independent H···π interactions, involving atoms H8*A* and H10*B* with average distances of 3.34 (12) and 3.21 (5) Å, from the six C atoms of the aromatic rings. On the other hand, in polymorph (II°) there are twice as many independent contacts classifiable as C—H···π, involving atoms H8*C*, H10*B*, H1*B* and H12*A* with average H—C distances significantly shorter, *i.e.* 3.02 (12), 3.04 (5), 3.01 (4) and 2.92 (5) Å. Finally, (iii) is due to the occurrence of N—H···N hydrogen bonds. The quite asymmetric appearance of fingerprint plots in form (II°) with respect to form (I) mirrors the asymmetries in the packing of the individual moieties in the asymmetric unit of this crystal form. As an example, in the plot of molecule *A* [form (II°)], only one lateral green spike is clearly visible below the main diagonal, at minimum d_i, $d_e \simeq 1.3$, 0.9 Å. A similar quasi-symmetrical spike is also visible above the diagonal, but it is shorter and thinner. This indicates that the N atoms of this molecule act mainly as acceptors of hydrogen bonds, whereas just the opposite is true when molecules *B* and *C* in the same form are considered (note that for the latter the thicker lateral spike falls above the main diagonal at d_i, $d_e \simeq 0.9$, 1.3 Å, *i.e.* in the region of the contacts by hydrogen-bond donors). Besides, these asymmetries signal that hydrogen-bonded pairs are formed between crystallographically non-equivalent units.

On the other hand, fingerprint plots of form (I) look more similar to each other, reflecting a more similar packing environment of the independent molecules in this phase with respect to the former. When the graphics of molecules *A* and *B* are compared between the two crystal forms, some differences emerge. As an example, in form (I) the lateral spikes indicative of hydrogen bonding are, on average, less evident. Table 2 displays the N—H···N intermolecular interactions in the asymmetric unit of the two polymorphs. In both forms, two independent N3*A*—H3*AN*···N3*B* and N3*B*—H3*BN*···N1*A* contacts are set up, but it is clear that those in crystal form (II°) are somewhat more favourable in terms of geometric parameters, with N—H···N angles closer to 180° and H···N distances equal or even shorter with respect to the other crystal form. Interestingly, the third independent molecule *C* in form (II°) makes a N3*C*—H3*CN*···N3*A* interaction with molecule *A*, which is absolutely the most favourable on purely geometrical grounds. Anyway, this contact could hardly be defined as a 'strong' hydrogen bond when compared with other similar interactions in the literature (see, as an example, Hsu & Craven, 1974).

It is interesting to note that a new feature appears only in the plot relative to molecule *A* in

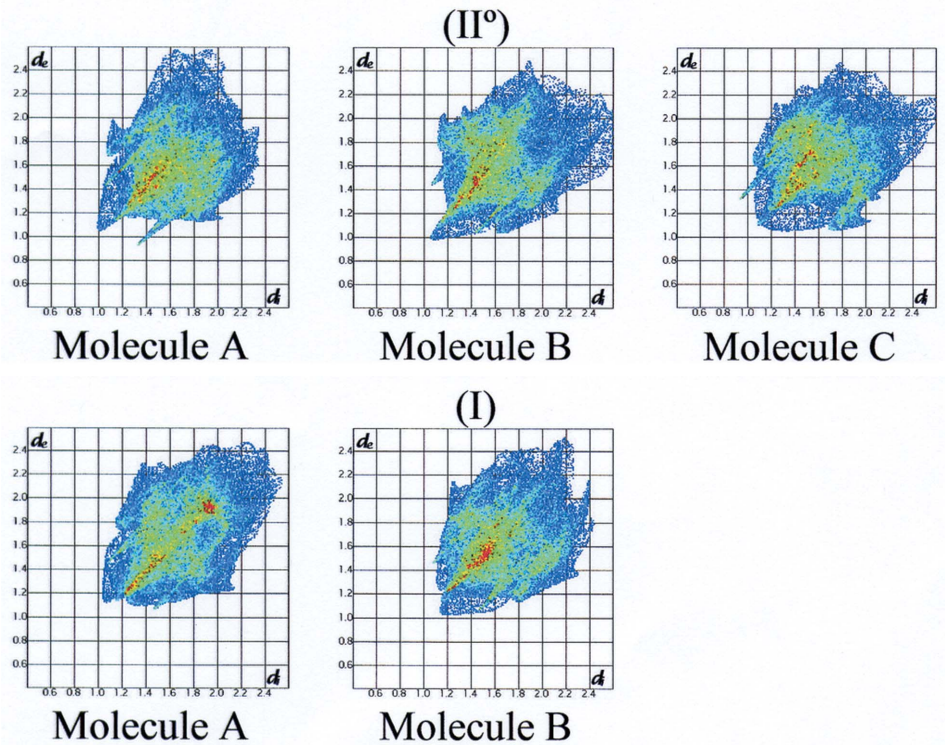

Figure 7
Hirshfeld surface fingerprint plots of the nearest internal distance (d_i) *versus* the nearest external distance (d_e) (Spackman & McKinnon, 2002) for each of the independent molecules in the two polymorphs of DIEN. The colours represent the number of points which share the same d_i, d_e coordinate (hot colours: many; cold colours: few). The graphics have been produced using *Crystal Explorer* 2.1 (Wolff *et al.*, 2007).

Table 2
N—H···N intermolecular contacts in DIEN polymorphs.

All the N—H···N contacts with $d_{H\cdots A}$ below 3.0 Å and with a bond angle greater than 120° are displayed. The complete list of intermolecular contacts involving H atoms, including C—H···N, can be found in the supplementary material (Table S2).

Reference molecule	Contact	d_{N-H} (Å)†	$d_{N\cdots N}$ (Å)	$d_{H\cdots N}$ (Å)	$\alpha_{N-H\cdots N}$ (°)	Symmetry‡
Form (II°)						
A	N3*A*—H3*AN*···N3*B*	1.013	3.581 (3)	2.709	144.3	$1-x,-y,2-z$
B	N3*B*—H3*BN*···N1*A*	1.014	3.411 (3)	2.521	146.3	$-1+x,y,z$
C	N3*C*—H3*CN*···N3*A*	1.016	3.251 (3)	2.264	163.6	$x,y,-1+z$
Form (I)						
A	N3*A*—H3*AN*···N3*B*	1.013	3.547 (2)	2.706	140.5	x,y,z
B	N3*B*—H3*BN*···N1*A*	1.014	3.448 (2)	2.549	147.6	x,y,z

† Covalent N—H distances derived from a gas-phase optimization at the B3LYP 6-311++G(p,d) theory level of the hydrogen coordinates (see text). ‡ Symmetry operation generating the acceptor atom, with translations expressed in terms of unit cell axes as reported in the deposited CIF file.

phase (I), *i.e.* quite a small red spot along the main diagonal at $d_i = d_e \simeq 1.9$ Å, *i.e.* at $d_i + d_e \simeq 3.8$ Å. It arises from significant overlap between parallel phenyl fragments and marks the occurrence of $\pi\cdots\pi$ interactions (Spackman & McKinnon, 2002). This contact involves the phenyl in molecule *A* and the inversion-related, exactly parallel group of the same molecule at $2-x,1-y,2-z$. The two fragments are slightly shifted with respect to each other, the average C···C distance between the two groups being as large as 3.833 (6) Å, which is to be compared with the orthogonal distance between the two six-membered ring planes (3.63 Å).

In §3.3 all these findings will be rationalized by the energy analysis of the DIEN polymorphs.

3.3. Comparison of the two polymorphic forms: energetics

3.3.1. Cohesive energies. Table 3 summarizes the crystal binding and cohesive energies of the two DIEN polymorphs, together with the relaxation and BSSE contributions. The crystal binding energy depends on all the attractive and repulsive interactions of a molecule with its crystalline environment, and it can be considered as a valuable overall indicator of the relative stability of each independent chemical unit in the crystal. Interestingly, in form (II°) both the crystal binding and the relaxation energies are virtually identical between the *endo* molecules *A* and *B*, while they differ markedly for the *exo* molecule *C*. With regard to form (I), it is worth noting that the individual crystal binding energies are more negative than those in form (II°). Nevertheless, on the basis of the total (BSSE uncorrected) binding energies E_b, polymorph (II°) turns out to be more stable than (I), in agreement with the density rule, which states that the most stable polymorph (*i.e.* that with the lowest energy at 0 K) should exhibit the most dense crystal packing. As a matter of fact, form (II°) of DIEN is ∼3% more dense than form (I) (see Table 1). It should be noted, however, that exceptions are possible when structures with different Z' or with important conformational differences among the molecules in the asymmetric unit are compared (Braun *et al.*, 2008), so the fulfilling of the rule should be considered as a sufficient condition to establish the order of the thermodynamic stability of a given substance. Anyhow, it should also be remarked that phase (II°) is the last appearing one, *i.e.* it forms when crystalline DIEN in phase (I) is left free to equilibrate with the mother solution at room temperature. In other words, polymorph (II°) grows under thermodynamic control as expected for a more stable phase. It should also be remarked that other DIEN polymorphs, even more stable than (II°), may still be found. All we can say is that the above cited experimental evidence, supported by the theoretical energy outcomes, suggests that phase (II°) is more stable with respect to (I).

The relaxation terms, E_{rel}, are important in both crystal forms, as should be expected for this highly flexible system. It has to be remarked that in DIEN E_{rel} is comparable with the binding energy, so it is not surprising that when they are accounted for the total crystal cohesive energy E_c turns out to be negligible in both crystal forms. Moreover, when the relaxation correction is taken into account, E_c turns out to be more stabilizing in polymorph (I), which is not in agreement with the above commented E_b results (Table 3). This is due to the extra contribution of the third independent molecule *C*, which is not present in form (I) and bears the greatest E_{rel} value (−34.11 kJ mol^{-1}).

The study of the conformational changes between the solid state and the gas-phase relaxed geometries are important in highlighting the zones of the molecule which are more affected by the crystal field. With regard to molecule *C* of form (II°), the most important alteration involves the lateral imine chains, which become ∼0.1–0.2 Å closer to each other in the most stable gas-phase geometry. Upon optimization the imine *exo* conformation of the macrocycle is preserved: the displacement of the lateral chains is due to a change in the relative orientation of the imidazolidine group with respect to the phenyl moiety and the lateral $-CH_2-CH_2-N=$ group (see Fig. S1 of the supplementary material). With regard to molecules *A* and *B*, the imidazolidine ring still rotates with respect to its attached phenyl and Schiff-base groups, although to a lesser extent when compared with molecule *C*; on the contrary, the most significant geometry changes involve rotations of the phenyls relative to the imine moieties.

The BSSE correction term, E_{BSSE}, is very large in the DIEN polymorphs and its average value amounts to 52 (2) kJ mol^{-1} per molecule in the solid state. Consequently, when this term is also considered, the total crystal binding and cohesive energies become positive. This is likely to be a consequence of the absence of the dispersive term in the DFT Hamiltonian (see §2). In other words, the major contribution to the solid-state

Table 3
Crystal cohesive energies (kJ mol^{-1}) of the DIEN polymorphs (II°) and (I).

	Molecule	(II°)	(I)
Crystal binding energy†	*A*	−16.87 (+41.02)	−24.01 (+25.93)
	B	−16.52 (+33.32)	−30.54 (+22.06)
	C	−44.48 (+3.77)	
Relaxation energy, E_{rel}‡	*A*	−17.95	−16.54
	B	−17.86	−23.16
	C	−34.11	
Total crystal binding energy, E_b§		−77.87 (+78.10)	−54.55 (+47.99)
Total crystal cohesive energy, E_c¶		−7.95 (+148.02)	−14.95 (+87.60)

† With E_{bulk} as the total crystal energy per unit cell, the binding energy was computed by the difference between the average energy per molecule E_m [*i.e.* $E_{bulk}/3$ in form (II°) and $E_{bulk}/2$ in form (I)] and the corresponding energy of the isolated molecule at the same level of theory, E_{iso}. The corresponding values after correction for BSSE are reported in parentheses. ‡ Computed by gas-phase calculations at the 6-311++G(p,d) DFT B3LYP theory level by the difference between the energy of the fully optimized molecular geometry and the energy of the isolated molecule at the same geometry employed in the solid-state calculations. § This term was evaluated as $E_b = E_{bulk} - \Sigma E_{iso}$, with the index of the summation running on all the molecules in the unit cell. Values corrected for BSSE are in parentheses. ¶ This term was evaluated as $E_c = E_b - \Sigma E_{rel}$, with the index of the summation running on all the molecules in the unit cell. Values corrected for BSSE are in parentheses.

Table 4
Dispersion contributions to the crystal cohesive energy for the independent DIEN molecules in the two polymorphs.

All values are given in kJ mol^{-1} and were computed by a summation of atom–atom potentials among each pair of different molecules located within ± 5 unit-cell translations in all directions around the reference cell.

	Molecule	*A*	*B*	*C*
Dispersion energy, E_{dis}†	(II°)	−301.63	−288.64	−285.30
	(I)	−281.36	−267.48	
Total contributions E_{dis}	(II°)	−875.57		
	(I)	−548.84		

† Dispersion potentials by Williams & Cox (1984); $E_{dis} = -(c_i\, c_j)^{1/2}/R^6$.

stability of this compound is just from the van der Waals attractive interactions. This was not unexpected: DIEN has no net dipole moment because of its intrinsic C_i point symmetry, nor strong hydrogen-bonded networks (see above).

3.3.2. Dispersion energies. To gain deeper insight into the dispersion contribution to the total cohesive energy, the total dispersion energies in the solid state have been evaluated through a summation of atom–atom empirically derived potentials (Williams & Cox, 1984) for the independent molecules of both polymorphs. Full details on the algorithm used can be found in the supplementary material. If the corresponding results reported in Table 4 are considered, it is clear that the dispersion energies, E_{dis}, always provide an important stabilizing contribution and that they are all considerably smaller in form (I). This indicates that in this polymorph, on average, there are weaker interactions. Interestingly, in phase (II°) the dispersion contributions to the interaction energy are very similar for all the three independent molecules, despite the fact that molecule *C* has a very different conformation and packing. Moreover, it should be noted that the greatest E_{dis} is always from molecule *A* in both polymorphs.

A tentative correction for the missing dispersion interactions can be made by adding the E_{dis} energies calculated within this empirical method (values in the last two rows in Table 4) to the total DFT, BSSE-corrected cohesive energy E_c (last row in Table 3). Results as low as −727.55 and −461.24 kJ mol^{-1} are obtained in this way as estimates of the overall crystal cohesive energies for polymorphs (II°) and (I). It can be concluded that the present calculations find form (II°) to be the most stable, as anticipated from the quantum mechanical, uncorrected binding energies (Table 3). This may indicate that forms (II°) and (I) are enantiotropically related (Herbstein, 2006), as the former is more stable but also has a lower melting point (440.5 *versus* 452.5 K, see Table 1). Anyhow, it should be remembered that the latter calculations are approximations of the true thermodynamic crystal stability, and must be considered as tools for ranking the energetics of the two polymorphs on a relative scale.

3.3.3. Intermolecular interaction energies. If a more detailed analysis of the relative importance of the intermolecular interactions is desired, a closer inspection of the relevant molecular pairs is in order. Table 5 shows the total interaction energies, E_{int}, of some isolated molecular pairs at the experimental solid-state geometry. Actually, if such pairs are strongly bonded in the vacuum, it is likely that they also provide an important contribution to the overall crystal stability. Each of them is made up of a crystallographically independent molecule and its next-nearest neighbour at various centre-of-mass distances (see Fig. S2 of the supplementary material). Analogous to the previous discussion on the periodic DFT results, for the isolated pairs the BSSE correction is quite large and comparable to the total interaction energy. With regard to polymorph (II°), as an example, E_{BSSE} ranges from $\sim$2 kJ mol^{-1} in the *A*–*A* pair to $\sim$11 kJ mol^{-1} in the *A*–*B* pair. With the exception of the strongly bonded *A*–*C* couple, accounting for the BSSE would provide repulsive interaction energies for all the molecular pairs considered, resulting therefore in scarcely informative energy estimates. This was not truly surprising: as previously pointed out, the most important term accounting for the crystal stability is dispersive; in other words, it is the E_{dis} contribution coming from the entire lattice which is responsible for joining together in the solid state the DIEN pairs which otherwise would depart from each other when isolated. Therefore, in Table 5 we report both the quantum mechanical, uncorrected total interaction energy and the empirical dispersion estimate as separate terms: then, such results will be correlated to the packing features discussed above.

In the solid state the closest-packed pair is the *A*–*B* one (see Figs. 6*c* and *d*); for this pair the uncorrected quantum-mechanical interaction energy is negative in both phases (II°) and (I). It should be remembered that, as previously discussed, molecules *A* and *B* are part of the *A*, *B*, *A*, *B* motif along the $\sim$12 Å long cell edge in both polymorphs. Indeed, this pair is

Table 5
Intermolecular interaction energies of the relevant isolated DIEN molecular pairs at the experimental geometry of the two polymorphs.

First row: quantum-mechanical total interaction energies, uncorrected for BSSE, evaluated by subtracting the energy of isolated molecules from the total energy of each molecular pair at the experimental geometry. All the calculations have been performed at the 6-311++G(p,d) DFT B3LYP theory level. The BSSE contribution ranged from ~ 2 to ~ 10 kJ mol^{-1} (see text). Second row: empirically derived (Williams & Cox, 1984) dispersion contribution, E_{dis}, to the molecular pair energy. Third row: geometric distance between the molecular centres of mass. All the quantities are given as kJ mol^{-1} and Å.

Molecular pair	*A*–*B*	*A*–*C*	*B*–*C*	*C*–*C*	*A*–*A*	*B*–*B*
(II°)	−1.96	−8.91	+2.97	+1.09	+3.54	−0.39
	−123.64	−40.24	−58.63	−18.27	−26.14	−12.29
	6.12	9.76	9.07	9.70	9.70	9.70
(I)	−2.75	–	–	–	+3.41	+7.13
	−119.52	–	–	–	−50.03	−39.68
	6.05	–	–	–	9.82	9.82

very similar in the two crystal forms (see Fig. S2 of the supplementary material): it involves just the same intermolecular H···N interactions, *i.e.* N3*A*—H3*AN*···N3*B*, N3*B*—H3*BN*···N1*A* (see Table 2) plus four weaker CH···N interactions (see Table S2 in the supplementary material). It is also worth noting that the contact geometry of this pair is preserved in all three solvated forms (see below and Fig. S4 of the supplementary material). Unavoidable differences in atomic positions result, sometimes, in the disappearance of a certain number of weak CH···N contacts, as their CHN angle or their H···N distance falls over the selected geometrical cut-offs. Anyhow, it should be remarked that all the two stronger NH···N interactions are always present within the *A*–*B* couple in all the DIEN crystal forms, no matter if they are solvated or not. Moreover, in both the unsolvated forms the dispersion contribution to the interaction energy of this pair was the greatest (Table 5), being $\sim$ 2–6 times larger than the same term reported for all the other pairs. It can be concluded that the *A*–*B* system constitutes a tightly bound aggregate, acting as a ubiquitous supramolecular synthon (as specified by Desiraju, 1995, 2007) in determining the crystal structure of all the known DIEN forms.

With regard to the other pairs in phase (II°), it is worth noting that it is *A*–*C* rather than *A*–*B* that shows the most stabilizing uncorrected quantum mechanical interaction energy. This is due to the favourable interaction geometry of the *A* and *C* molecules in the solid state, and it should be remembered that in this polymorph molecule *C* has the uncommon *exo* conformation. The only other form of DIEN that has three independent molecules in the unit cell is SOLV: in this phase, the isolated *A*–*C* pair, which has molecule *C* arranged in the more common *endo* conformation, bears a small and positive (+0.71 kJ mol^{-1}) interaction energy (see Table S3 of the supplementary material). It is important to note that it is just the imine *exo* conformation of *C* in (II°) which allows the formation of the most favourable N3*C*—H3*CN*···N3*A* contact reported in DIEN (see Table 2 above). Moreover, comparing the fingerprint plots of *C* in (II°) (Fig. 7) and in SOLV (Fig. S3 of the supplementary material), it is clear that in the latter there are no significant CH···π interactions, whereas in the unsolvated phase a close C11*A*—H12*A*···π contact is set up among the methylene and the almost orthogonal phenyl plane of molecule *C*. It can be concluded that the *exo* arrangement of *C* in (II°) provides an overall stabilizing contribution, owing to the favourable intermolecular interactions with *A*, which in turn are completely missing in the solvated crystal form of the macrocycle. The other pairs (*B*–*C*, *C*–*C*, *A*–*A*), except *B*–*B*, are not stable in the gas phase; nevertheless, all the corresponding interactions for these couples are small and barely significant (Table 5).

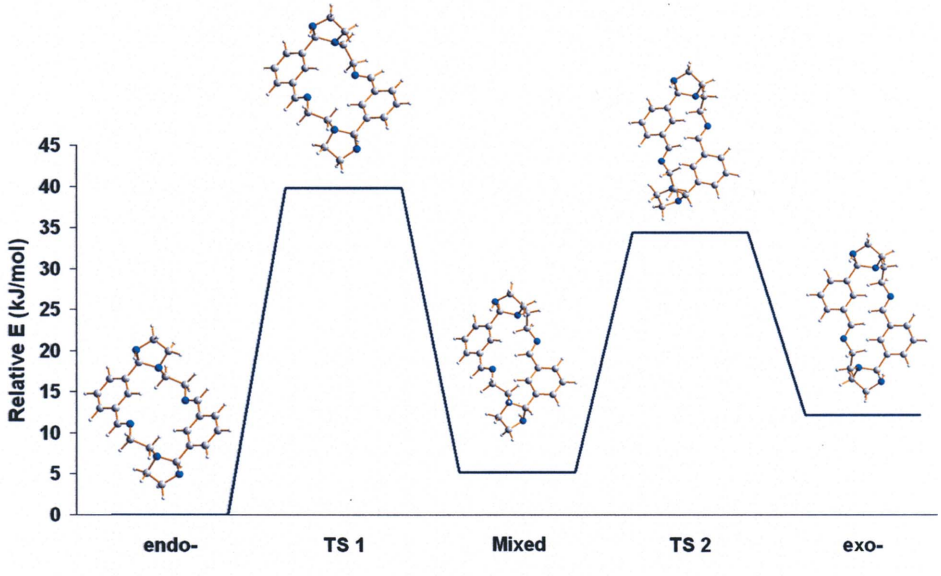

Figure 8
Gas-phase energetic profile (kJ mol^{-1}) at the 6-31G(d) B3LYP theory level *versus* the reaction coordinate between the imine *endo* and the immune *exo* conformations of the DIEN molecule, taking the energy of the *endo* conformer as the reference. This figure is in colour in the electronic version of this paper.

3.3.4. Study of the *endo*/*exo* interconversion mechanism. Fig. 8 reports the energetic trend of the gas-phase interconversion mechanism, entirely evaluated at the B3LYP 6-31G(d) theory level, between the *endo* and the *exo* conformations of DIEN. Details on the strategy of the optimization of the transition state, with some other comments, can be found in the supplementary material. We found a possible path for the *endo*

Table 6
Comparison among the relevant crystallographic and packing parameters of solvated forms of DIEN.

Refcode	Solvent†	a (Å)	b (Å)	c (Å)	α (°)	β (°)	γ (°)	V (Å^3)	Z, Z'	Space group	ρ (g cm^{-3})	m.p. range (K)
Crystallographic details												
SOVJUY‡	CH_2Cl_2	17.448 (21)	17.028 (24)	18.190 (23)	90	118.16 (9)	90	4765 (11)	8, 1	$C2/c$	1.181	429–431
KIGVEB§	CH_3OH	17.283 (2)	16.930 (2)	17.953 (3)	90	118.73 (2)	90	4607 (2)	8, 1	$C2/c$	1.207	Not rep.
SOLV¶	CH_3CN, H_2O	12.237 (1)	12.563 (1)	13.009 (1)	92.622 (3)	111.847 (3)	79.441 (3)	1824.4 (3)	3, 1.5	$P\bar{1}$	1.185	417

† Disordered solvent in the unit cell. ‡ Adams *et al.* (1991). § Menif *et al.* (1990). ¶ This work, with the cell axes setting differing from that reported in Table 1 and in the deposited CIF for the sake of comparison with the other two structures.

Intermolecular NH···N contacts†

Crystal form	Reference molecule	Contact	d_{N-H} (Å)	$d_{N\cdots N}$ (Å)	$d_{H\cdots N}$ (Å)	$\alpha_{N-H\cdots N}$ (°)	Symmetry
SOVJUI			1.009	3.794 (19)	2.928	144.4	$1-x, y, \frac{1}{2}-z$
KIGVEB	*A*	N3*A*—H3*AN*···N3*B*	1.009	3.798 (8)	2.935	144.1	$1-x, -y, -z$
SOLV			1.014	3.494 (4)	2.583	149.3	$x, 1+y, z$
SOVJUI			1.009	3.648 (16)	2.792	142.8	$1-x, y, \frac{1}{2}-z$
KIGVEB	*B*	N3*B*—H3*BN*···N1*A*	1.009	3.624 (7)	2.795	139.0	$1+x, y, z$
SOLV			1.015	3.371 (5)	2.475	146.9	$-x, 1-y, -z$
SOLV	*C*	N3*C*—H3*CN*···N1*B*	1.015	3.608 (4)	2.792	137.6	$1+x, y, z$

† Same quantities, with the same measure units and the same physical meaning, as in Table 2. According to the procedure followed for the two DIEN polymorphs, the H atoms have been relocated by partial optimization in the gas phase at the 6-311++G(p,d) B3LYP theory level. The complete list of CH···N is also reported in the supplementary materials (Table S4).

↔ *exo* interconversion which first involves the rotation of one of the two imine chains around the C5—C7 bond. This rearrangement results in a new conformer (hereinafter 'mixed'), with one imine N atom exhibiting the *exo* geometry, and the other the *endo* one. The mixed molecule has an energy intermediate between the pure *endo* and *exo* conformers, with the two phenyl groups no longer being parallel to each other. In the succeeding step the other imine lateral chain also rotates, so that both the imine groups adopt the final *exo* conformation. Owing to the C_i symmetry of the reactant and product, it is not important which lateral chain begins to rotate. From Fig. 8 it is worth noting that the imine *endo* conformer is 12.13 kJ mol^{-1} lower in energy with respect to the imine *exo* one, in agreement with the experimental evidence that the *endo* conformation is by far the most common one in the known solid-state forms of DIEN. The interconversion barrier height relative to the direct reaction (*endo* → mixed) amounts to 39.76 kJ mol^{-1} (9.50 kcal mol^{-1}), while the same barrier for the inverse process (mixed → *endo*) is a bit smaller (34.52 kJ mol^{-1}, *i.e.* 8.25 kcal mol^{-1}). On the contrary, the barriers for the mixed ↔ *exo* process are 29.12 kJ mol^{-1}, *i.e.* 6.96 kcal mol^{-1} (direct) and 22.23 kJ mol^{-1}, *i.e.* 5.31 kcal mol^{-1} (inverse). It should be noted that other interconversion paths are possible. The mechanism proposed here is not exclusive, as other high-energy minima could be located on the potential energy surface (PES) between the two final *endo* and *exo* conformations. Nevertheless, the complete study of the PES of DIEN goes far beyond the purpose of this work, which mainly aims to provide an estimate of the height of the *endo* ↔ *exo* interconversion barriers.

The difference between the energy of the transition states and that of the gas-phase minima never exceeds 41.87 kJ mol^{-1} (10 kcal mol^{-1}), therefore, at ordinary temperatures it is quite easy for the system to climb the *endo*/*exo* barriers. This implies that even in solution a certain amount of the *exo* conformer could be present. It should be noted that the formation of such a conformer is a necessary condition for the growth of phase (II°), which is the most stable from empirical evidence and theoretical estimates (see above). Such findings agree well with the so-called 'Ostwald's rule: as stated by Ostwald at the end of 19th century (Ostwald, 1897), '*when leaving a metastable state, a given chemical system does not seek the most stable one, rather the nearest metastable one that can be reached with the minimum loss of free energy*'. In other words, the first appearing polymorph is not the most stable, but rather the one able to crystallize most quickly (I). Subsequently, if the solid is left free to equilibrate with the surrounding solution, the thermodynamically most stable form (II°) appears.

3.4. Solvated structures

It is not uncommon that organic substances even of medium to low molecular weight include solvent in their crystal structure: in the 2009 release of the CSD, 8.5% of the total organic structures contain some crystallization solvent, which is moreover disordered in 6.1% of cases. Furthermore, it is known that compounds that crystallize with $Z' > 1$ tend to form co-crystals more easily than compounds which exhibit $Z' = 1$ in their pure form (Anderson *et al.*, 2008). The chemical nature of solvent and/or additives plays a key role in the growth of the solid phase (Thallapally *et al.*, 2004; Day *et al.*, 2006), being one of the most significant factors which determine the final product of the crystallization process. However,

until now the underlying reasons for which a certain solvent influences the crystal growth in a certain way are, generally speaking, understood very little: the trial-and-error method is still the most valuable to obtain new polymorphs, whose appearance is in most cases unexpected (Day *et al.*, 2006). Nevertheless, such reasons must reside in the interactions between the solvent and the molecules themselves. The study of different solvated forms of the same substance may therefore be important to provide a rationale of the interplay among heteromolecular interactions, conformation and observed crystal packing.

With regard to the present case, apart from the SOLV phase (acetonitrile/water solvate) presented here for the first time, in the literature two other solvated DIEN forms are known (Menif *et al.*, 1990; Adams *et al.*, 1991: see also §3.1), containing methanol or dichloromethane. Table 6 outlines a synoptic comparison of these three DIEN solvated forms from a crystallographic and packing perspective, while Fig. 9 displays the superposition of their packing arrangements. It should be noted that quite different crystallization procedures were employed to obtain such forms. KIGVEB (methanol solvate) was grown by slow solvent evaporation over a period of 3 d from a 1:1 CH_3OH/CH_3CN solution (Menif *et al.*, 1990), while SOLV was obtained by abruptly cooling a CH_3CN (excess):CH_2Cl_2 solution (see above). Less details are given for SOVJUI (dichloromethane solvate; Adams *et al.*, 1991), only that it was '*recrystallized from a dichloromethane/acetonitrile mixture*'. Curiously, all the reported methods use, in different conditions, acetonitrile as part of the crystallization mixture, but SOLV is the unique form which includes this solvent in the crystal structure.

It is quite evident that the KIGVEB and SOVJUI forms are very similar to each other, both of them sharing the same space group, $C2/c$, in disagreement with SOLV which crystallizes as $P\bar{1}$. Moreover (see Table 6), KIGVEB and SOVJUI have a cell volume which is considerably greater with respect to SOLV. Another important difference among these forms lies in the composition of the asymmetric unit: SOLV contains *three* half DIEN molecules ($Z' = 1.5$), as in the unsolvated form (II°), while KIGVEB and SOVJUI are composed of *two* half molecules, resulting in an overall $Z' = 1$ as in the unsolvated form (I).

Notwithstanding the differences highlighted above, some important similarities can be found:

(i) All the three structures are centrosymmetric, so the C_i molecular point symmetry is always preserved.

(ii) The density of the three solvated forms is quite similar (see Table 6), with the KIGVEB structure being 1.6% more dense than SOLV, which in turn is only 0.3% more dense than SOVJUI.

(iii) None of the three solvated forms contain the *exo* conformer: in SOLV the third independent molecule shows the most common *endo* conformation (see above).

(iv) The three structures all show the same basic *A*, *B*, *A*, *B* packing motif described earlier (see Fig. 9), and the *A*–*B* molecular pair is very similar in all the DIEN crystal forms, irrespective of whether they are solvated or not (see Figs. S2 and S4 of the supplementary material and the discussion in §3.3.3).

The Hirshfeld surface fingerprint plots were again employed to compare the overall packing features of the solvated phases. A full discussion based on such plots can be found in the supplementary material. Here we conclude that the main packing features, such as H···H contacts, hydrogen bonds and C—H···π interactions, are common to both solvated and unsolvated forms. In general, differences in the fingerprint plots can be classified as being due to the nature of the solvent or to the crystal symmetry. The former are relative to features specific to DIEN···solvent interactions, recognizable as they appear only if a certain solvent is included in the

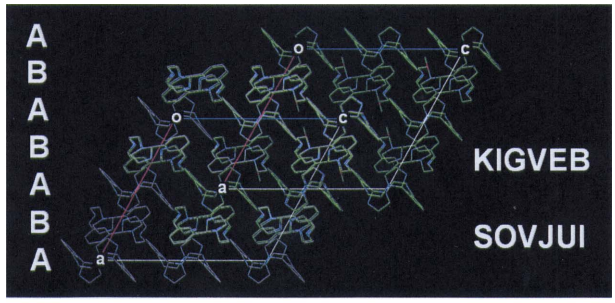

(*a*)

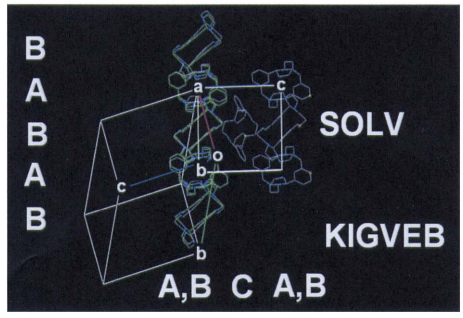

(*b*)

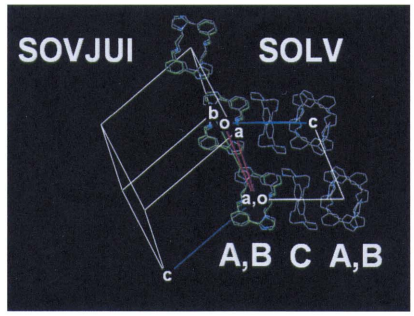

(*c*)

Figure 9
Packing motifs of the known solvated forms of DIEN. (*a*) Comparison between the two forms reported in the CSD. Grey molecules: SOVJUI (methanol solvated). Green molecules: KIGVEB (dichloromethane solvate). Both unit cells are viewed down the *b* axis. (*b*) Same as (*a*), with the comparison made between the acetonitrile/water solvated SOLV form (grey molecules) and the KIGVEB structure (green molecules). The SOLV unit cell is drawn along the *a* axis. (*c*) Same as (*a*) and (*b*), with the structures compared being the SOLV form (grey molecules, viewed down the *b* axis) and the SOVJUI form (green molecules). This figure is in colour in the electronic version of this paper.

structure. Also belonging to this category is, for example, the large and broad spike in SOVJUI at the minimum $d_i + d_e \simeq 0.7 + 1.3$ Å (molecule *A*), which is due to H···Cl contacts with dichloromethane and is missing both in KIGVEB and SOLV. The differences due to crystal symmetry, on the other hand, are specific to a certain space group and do not depend on the chemical nature of the co-crystallized solvent. As an example, both the methanol and the dichloromethane solvates (*C*2/*c*) show T-shaped phenyl–phenyl long contacts (see supplementary material), which do not appear in the $P\bar{1}$ structures.

A crucial point to be noted is that in all the solvated forms the solvent is disordered to some extent. In KIGVEB the methanol molecule lies near a *c* glide plane and it was modelled employing a fixed 50% occupancy in the final crystallographic refinement (Menif *et al.*, 1990). In SOVJUI, CH_2Cl_2 is positioned across a crystallographic C_2 axis and in the original work it was treated as disordered with fixed low occupancy (0.25 per molecule; Adams *et al.*, 1991). In SOLV, a disordered model was employed only for the CH_3CN methyl, with final occupancy factors estimated to be as high as 0.54 (3) and 0.46 (2) for its two accessible positions. Moreover, in the final refinement a disordered, single water molecule with an occupancy as large as 0.342 (7) was placed in a different zone in the unit cell to account for quite a large residual Fourier peak near H14*C* (see supplementary material for a complete discussion). It should be noted that the amount of solvent per cell is considerably lower in the SOLV form [2.68 (1) moles per cell, adding acetonitrile and water] with respect to KIGVEB (which contains 8 formula units per cell) and SOVJUI (4 formula units per cell). This evidence could justify the dramatic difference in crystal symmetry of such structures ($P\bar{1}$ *versus* *C*2/*c*), but it is hard to discriminate if this is truly due to the different nature of the solvent, or rather to the different crystallization conditions. From the present discussion it can be inferred that the main packing features, such as the strongly bonded *A*–*B* molecular pair and most of the intermolecular contacts, are essentially the same irrespective of the identity of the solvent. As an example, in all the three forms there are contacts such as C11*A*—H13*A*···*X* and C12*B*—H14*B*···*X* of similar geometry, where *X* can be water/methanol oxygen or even chlorine (see Table S4 of the supplementary material). Such a resemblance is impressive between KIGVEB and SOVJUI, despite the chemical dissimilarity of CH_3OH and CH_2Cl_2, as exactly the same kind of DIEN···solvent CH···*X* contacts are set up (see Table S4). On the contrary, other interactions which are not present in the latter forms emerge in SOLV (*i.e.* HOH···DIEN and DIEN···$NCCH_3$ hydrogen bonds) because of the presence of two different solvent species in the unit cell.

Inspecting the packing similarities among the three solvated phases described above, we believe that in the present case the observed crystal symmetry is mainly dictated by crystallization conditions, while the chemical nature of the solvent appears to play a less central role. In particular, the time invested in the crystallization appears to be by far the most striking factor, even if the composition of the crystallization mixture is also important in influencing the nucleation and growth kinetics. These suppositions are somewhat supported by evidence that the SOLV form has been obtained by ourselves from the same solution which would lead to (I) and (II°) by simply abruptly lowering the temperature. It could be interesting for future work to investigate if, tuning the crystallization conditions or the relative ratio of the solvents in the crystallization mixture, other phases may be obtained.

4. Conclusions

In this work we have presented three newly discovered solid phases of a Schiff-base organic ligand macrocycle, and we have compared our findings with two other solvated phases of the same substance known in the literature. The following conclusions can be drawn:

(i) In the solid state two distinct conformations of the DIEN molecules have been found. In the *endo* conformation the imine N atoms point towards the interior of the macrocycle. In the *exo* conformation the same imine N atoms are directed outside the macrocycle ring. The *endo* arrangement, which is ubiquitous in the solid state, is also the most stable in the gas phase by ~ 12 kJ mol^{-1}. The *exo* form, on the other hand, appears only in phase (II°), which contains both the conformers.

(ii) The independent molecules *A* and *B* in the same *endo* conformation constitute an invariant supramolecular synthon in all the DIEN crystal forms, including those reported in the literature (KIGVEB and SOVJUI). Such a molecular pair is greatly stabilized by dispersive interactions and is the building block of the alternating *A*, *B*, *A*, *B* stacks common to all the DIEN phases. The third independent molecule, *C*, which can assume both the *endo* (SOLV) or *exo* (II°) conformation, intercalates between the parallel columns made up by repeated *A*, *B* units. This in turn results in the lengthening of a cell edge and, correspondingly, a significant increase in cell volume.

(iii) From the inspection of the Hirshfeld surface fingerprint plots, it is clear that all the DIEN forms share similar packing features, such as C—H···π interactions and N—H···N hydrogen bonds, the latter being somewhat stronger in the unsolvated phase (II°). In form (I) quite long π···π contacts among the molecular pairs *A*–*A* emerge as a new feature, but they supply less important interaction energy contributions to the overall crystal stability with respect to those provided by the above-mentioned *A*–*B* pair.

(iv) The main stabilizing term to the crystal cohesive energy in DIEN crystal forms is dispersive, as can be expected from the lack of strong hydrogen-bond networks or electrostatic interactions involving odd-order moments. Polymorph (II°) was found to be the most stable one by periodic DFT calculations and dispersion energy estimates. It is worth noting that the *endo*/*exo* isolated molecular pair *A*–*C* in such a polymorph, which also bears the most favourable N—H···N interaction on purely geometrical grounds, is the most stabilized one from the quantum mechanical calculations. On the contrary, the similar *endo*/*endo* *A*–*C* isolated pair in SOLV has a weakly repulsive quantum mechanical energy.

(v) The solvated forms share essentially the same main packing features as described above, such as the strongly bonded *A*–*B* molecular pair and even most of the intermolecular contacts, irrespective of the identity of the solvent. Such a resemblance is impressive between KIGVEB and SOVJUI, despite the chemical dissimilarity of the co-crystallized CH_3OH or CH_2Cl_2. We attribute the difference in crystal symmetry among KIGVEB/SOVJUI and the newly discovered SOLV phase mainly to the different crystallization conditions, rather than to the chemical nature of the guest solvent(s).

These conclusions may also be correlated to the observed transformation of the DIEN samples during the crystallization procedure (see §2). In particular, the evidence that no interconversion occurs between (II°) and (I) when the samples are removed from their mother solution suggests that the solvent must play a fundamental role in setting the equilibrium between the two forms. It should be noted that if the temperature is abruptly lowered at the end of the synthesis process, only the forms SOLV (majority) and (I) (minority) appear. SOLV contains three independent molecules as (II°), but the third one, *C*, adopts the most common *endo* conformation. The appearance of the less stable *exo* conformer in the solid state, which on the contrary is associated with the most stable crystal phase, occurs only under thermodynamic control and it is hindered at lower temperatures due to the ~ 30–$40\ \mathrm{kJ\ mol^{-1}}$ high conformational barriers. Our estimates indicate that the interconversion between the two conformers is possible at room temperature, so it is likely that the *endo* $\leftrightarrow$ *exo* equilibrium is set up in solution. In other words, the system is brought towards the most stable polymorph by the thermodynamic driving force owing to the most favourable intermolecular interaction of the *exo* molecule *C* in its crystalline environment. On the basis of such experimental and theoretical findings, we infer that the interconversion between the two polymorphs takes place through a series of equilibria in solution such as

$$\begin{aligned} &\text{(I) (solid, } endo) \leftrightarrow \text{(solution, } endo) \\ &\text{(solution, } endo) \leftrightarrow \text{(solution, } endo + exo) \\ &\text{(solution, } endo + exo) \leftrightarrow \text{(II°) (solid, } endo + exo) \end{aligned} \quad (2)$$

rather than through a direct solid-state to solid-state transition (I) $\Rightarrow$ (II°). However, thermal DSC and TGA measurements are in order to complete an outline of this system and to provide fusion enthalpy data that could be correlated quantitatively with our energy estimates (which, on the contrary, only provide information on the stability of the various crystal forms on a relative scale). However, the scarce amount of material we obtained, especially for phase (I), did not allow for such investigations.

A concluding remark is worthy of note. Owing to the amount of relaxation and BSSE energies, together with the well known problem of modelling of the dispersive interactions in the solid state within the ground-state DFT methods, an accurate estimation of the quantum-mechanical crystal cohesive energies appears to be a very difficult task, even on a relative scale. As recently pointed out by Civalleri *et al.* (2007), '*the shortcoming of DF methods in describing dispersive forces and the spurious extra binding given by the BSSE dramatically hampers a proper prediction of the structure and stability*' of even simple molecular crystals such as the urea crystal. Nevertheless, even if post-Hartree–Fock methods have become recently available in the widely used periodic simulation software such as *CRYSTAL*09 (Dovesi *et al.*, 2009), it should be noted that until now they have been used to deal with only quite small systems (Erba *et al.*, 2010; Tsuzuki *et al.*, 2010). We believe that the computational effort required to apply such methods to molecules as large as DIEN in the solid state is at the moment overwhelming, especially considering that even correlated methods require adequately large basis sets to provide accurate results. As stated by Tsuzuki *et al.* (2010), '*the highly computationally demanding periodic MP2 and CCSD(T) calculations of large molecular crystals containing more than 20 heavy atoms in a unit cell are not practical at present*'. With regard to the present work, experimental findings provided not only the solid-state geometries to be used in the periodic single-point calculations, but also precious and crucial information for the correct interpretation of both DFT and empirical results. In particular, accurate surveillance of the crystallization process allowed us to hypothesize on the relative stability of the newly appearing phases, whereas the theoretical estimates of the interaction and cohesive energies allowed us to rationalize the observed macroscopic transformations of the DIEN crystals.

Thanks are due to Dr Mario Barzaghi (CNR-ISTM) for fruitful discussions. We also thank Mr Pietro Colombo and Dr Laura Loconte for technical assistance. Thoughtful comments by one of the reviewers and financial support from the Italian MIUR (Fondi PUR 2008) are also acknowledged.

References

Adams, H., Bailey, N. A., Fenton, D. E., Good, R. J., Moody, R. & Rodriguez de Barbarin, C. O. (1987). *J. Chem. Soc. Dalton Trans.* pp. 207–218.
Adams, H., Bailey, N. A., Fenton, D. E., Hempstead, P. D. & Westwood, G. P. (1991). *J. Incl. Phenom. Mol. Recognit. Chem.* **11**, 63–69.
Anderson, K. M., Probert, M. R., Whiteley, C. N., Rowland, A. M., Goeta, A. E. & Steed, J. W. (2008). *Cryst. Growth Des.* **9**, 1082–1087.
Becke, A. D. (1993). *J. Chem. Phys.* **98**, 1372–1375.
Bernstein, J. (1993). *J. Phys. D Appl. Phys.* **26**, B66–B76.
Bernstein, J. (2002). *Polymorphism in Molecular Crystals.* Oxford University Press.
Boys, S. F. & Bernardi, F. (1970). *Mol. Phys.* **19**, 553–566.
Brandenburg, K. (2010). *DIAMOND*, Version 3.2d. Crystal Impact GbR, Bonn, Germany, http://www.crystalimpact.com/diamond/.
Braun, D. E., Többens, D. M., Kahlenberg, V., Ludescher, J. & Griesser, U. J. (2008). *Cryst. Growth Des.* **8**, 4109–4119.
Civalleri, B., Doll, K. & Zicovich-Wilson, C. M. (2007). *J. Phys. Chem. B*, **111**, 26–33.
Clausen, H. F., Chevallier, M. S., Spackman, M. A. & Iversen, B. B. (2010). *New J. Chem.* **34**, 193–199.
Corradini, P. (1975). *J. Polym. Sci.* **51**, 1–6.
Day, G. M. *et al.* (2005). *Acta Cryst.* B**61**, 511–527.

Day, G. M. *et al.* (2009). *Acta Cryst.* B**65**, 107–125.
Day, G. M., Trask, A. V., Motherwell, W. D. S. & Jones, W. (2006). *Chem. Commun.* **1**, 54–56.
Desiraju, G. R. (1995). *Angew. Chem. Int. Ed Engl.* **34**, 2311–2327.
Desiraju, G. R. (2007). *Angew. Chem. Int. Ed.* **46**, 8342–8356.
Dobson, J. F., McLennan, K., Rubio, A., Wang, J., Gould, T., Lee, H. M. & Dinte, B. P. (2001). *Aust. J. Chem.* **54**, 513–527.
Dovesi, R., Saunders, V. R., Roetti, C., Orlando, R., Zicovich-Wilson, C. M., Pascale, F., Civalleri, B., Doll, K., Harrison, N. M., Bush, I. J., D'Arco, Ph. & LLunell, M. (2006). *CRYSTAL*06 *User's Manual.* University of Torino, Italy.
Dovesi, R., Saunders, V. R., Roetti, C., Orlando, R., Zicovich-Wilson, C. M., Pascale, F., Civalleri, B., Doll, K., Harrison, N. M., Bush, I. J., D'Arco, Ph. & LLunell, M. (2009). *CRYSTAL*09 *User's Manual.* University of Torino, Italy.
Drew, M. G. B. (1980). *J. Chem. Soc. Dalton Trans.* pp. 1678–1684.
Erba, A., Pisani, C., Casassa, S., Maschio, L., Schütz, M. & Usvyat, D. (2010). *Phys. Rev. B*, **81**, 165108.
Fabbiani, F. P. A., Allan, D. R., Parsons, S. & Pulham, C. (2005). *CrystEngComm*, **7**, 179–186.
Frisch, M. J. *et al.* (2004). *GAUSSIAN*03, Revision C.02. Gaussian Inc., Wallingford, CT, USA.
Frisch, M. J. *et al.* (2009). *GAUSSIAN*09, Revision A.1. Gaussian, Inc., Wallingford CT, USA.
Gatti, C., Saunders, V. R. & Roetti, C. (1994). *J. Chem. Phys.* **101**, 10686–10696.
Herbstein, F. H. (2006). *Acta Cryst.* B**62**, 341–383.
Hsu, I.-N. & Craven, B. M. (1974). *Acta Cryst.* B**30**, 988–993.
Kofler, L. & Kofler, A. (1954). *Thermo-Mikro-Methoden zur Kennzeichnung organischer Stoffe und Stoffgemische*, p. 467. Weinheim: Verlag Chemie.
Lee, C., Yang, W. & Parr, R. G. (1988). *Phys. Rev. B*, **37**, 785–789.
Lommerse, J. P. M., Motherwell, W. D. S., Ammon, H. L., Dunitz, J. D., Gavezzotti, A., Hofmann, D. W. M., Leusen, F. J. J., Mooij, W. T. M., Price, S. L., Schweizer, B., Schmidt, M. U., van Eijck, B. P., Verwer, P. & Williams, D. E. (2000). *Acta Cryst.* B**56**, 697–714.
Lo Presti, L., Ellern, A., Destro, R. & Lunelli, B. (2009). *J. Phys. Chem. A*, **113**, 3186–3196.
Ma, H., Allmendinger, M., Thewalt, U., Lentz, A., Klinga, M. & Rieger, B. (2002). *Eur. J. Inorg. Chem.* pp. 2857–2867.
Martell, A. E., Motekaitis, R. J., Menif, R., Rockcliffe, D. A. & Llobet, A. (1997). *J. Mol. Catal. A Chem.* **117**, 205–213.
McCrone, W. C. (1965). *Polymorphism in Physics and Chemistry of the Organic Solid State*, edited by D. Fox, M. M. Labes & A. Weissberger, Vol. II, pp. 726–767. New York: Wiley Interscience.
McKinnon, J. J., Mitchell, A. S. & Spackman, M. A. (1998). *Chem. Eur. J.* **4**, 2136–2141.
Menif, R. & Martell, A. E. (1989). *J. Chem. Soc. Chem. Commun.* pp. 1521–1523.
Menif, R., Martell, A. E., Squattritto, P. J. & Clearfield, A. (1990). *Inorg. Chem.* **29**, 4723–4729.
Moggach, S. A., Allan, D. R., Parsons, S. & Sawyer, L. (2006). *Acta Cryst.* B**62**, 310–320.
Moggach, S. A., Parsons, S. & Wood, P. A. (2008). *Crystallogr. Rev.* **14**, 143–184.
Motherwell, W. D. S. *et al.* (2002). *Acta Cryst.* B**58**, 647–661.
Mourik, T. van & Gdanitz, R. J. (2002). *J. Chem. Phys.* **116**, 9620–9623.
Nangia, A. (2008). *Acc. Chem. Res.* **41**, 595–604.
Neumann, M. A., Leusen, F. J. J. & Kendrick, J. (2008). *Angew. Chem. Int. Ed.* **47**, 2427–2430.
Ostwald, W. (1897). *Z. Phys. Chem.* **22**, 289–330.
Rohl, A. L., Moret, M., Kaminsky, W., Claborn, K., McKinnon, J. J. & Kahr, B. (2008). *Cryst. Growth Des.* **8**, 4517–4525.
Seddon, K. R. (2004). *Cryst. Growth Des.* **4**, 1087.
Spackman, M. A. & McKinnon, J. K. (2002). *Cryst. Growth Des.* **66**, 378–392.
Spackman, M. A. & Mitchell, A. S. (2001). *Phys. Chem. Chem. Phys.* **3**, 1518–1523.
Steiner, T. (2000). *Acta Cryst.* B**56**, 673–676.
Thallapally, P. K., Jetti, K. R., Katz, A. K., Carrell, H. L., Singh, K., Lahiri, K., Kotha, S., Boese, R. & Desiraju, G. R. (2004). *Angew. Chem. Int. Ed.* **43**, 1149–1155.
Threlfall, T. L. (1995). *Analyst*, **120**, 2435–2460.
Trask, A. V., Shan, N., Motherwell, W. D. S., Jones, W., Feng, S., Tan, R. B. H. & Carpenter, K. J. (2005). *Chem. Commun.* pp. 880–882.
Tsuzuki, S., Orita, H., Honda, K. & Mikami, M. (2010). *J. Phys. Chem. B*, **114**, 6799–6805.
Utz, D., Heinemann, F. W., Hampel, F., Richens, D. T. & Schindler, S. (2003). *Inorg. Chem.* **42**, 1430–1436.
Williams, D. E. & Cox, S. R. (1984). *Acta Cryst.* B**40**, 404–417.
Wolff, S. K., Grimwood, D. J., McKinnon, J. J., Jayatilaka, D. & Spackman, M. A. (2007). *CrystalExplorer 2.1*. University of Western Australia. See also http://www.hirshfeldsurface.net.